Desalination and Water Treatment
www.deswater.com

doi: 10.5004/dwt.2019.24068

154 (2019) 312–319
June

Pt/g-C_3N_4 composites for photocatalytic H_2 production and •OH formation

Kezhen Qi[a,b], Shu-yuan Liu[c,f,*], Ruidan Wang[a,*], Zhe Chen[d,*], Rengaraj Selvaraj[e]

[a]*Institute of Catalysis for Energy and Environment, College of Chemistry and Chemical Engineering, Shenyang Normal University, Shenyang 110034, China, emails: wangruidan1980@163.com (R. Wang), qkzh2003@aliyun.com (K. Qi)*
[b]*Key Laboratory of Advanced Energy Materials Chemistry (Ministry of Education), Nankai University, Tianjin, 300071, China*
[c]*Department of Pharmacology, Shenyang Medical College, Shenyang 110034, China, email: liushuyuan@symc.edu.cn*
[d]*School of Material Science and Technology, Jilin Institute of Chemical Technology, Jilin 130010, China, email: chenzhecz999@163.com*
[e]*Department of Chemistry, College of Science, Sultan Qaboos University, Muscat 123, Sultanate of Oman, email: srengaraj1971@yahoo.com*
[f]*Key Laboratory for Photonic and Electronic Bandgap Materials, Ministry of Education, School of Physics and Electronic Engineering, Harbin Normal University, Harbin 150025, China*

Received 27 October 2018; Accepted 1 March 2019

ABSTRACT

A simple method has been reported to prepare the Pt/g-C_3N_4 composites with different loading amount of Pt nanoparticles (NPs). These Pt/g-C_3N_4 composites have a better photocatalytic performance than pure g-C_3N_4 offering for water splitting into hydrogen. The Pt NPs are uniformly spread on g-C_3N_4 surfaces, with their diameters in the range of 4–8 nm. Loading of Pt NPs can expand the response of visible light for g-C_3N_4 and reduce the recombination rate of photogenerated carriers. Therefore, the performance of water splitting into hydrogen via g-C_3N_4 photocatalysis under sunlight is enhanced by using the cocatalyst of Pt. Pt/g-C_3N_4 (3 wt.% of Pt) shows the highest activity (841 μmol g^{-1} h^{-1}) among the as-prepared samples, while the pure g-C_3N_4 almost no hydrogen production. This work demonstrates that the Pt/g-C_3N_4 composite is one of potential photocatalysts for hydrogen generation.

Keywords: g-C_3N_4; Pt nanoparticles; Photocatalysis; Water splitting; H_2 production

1. Introduction

With the population growth and industry development, energy crisis and environmental pollution threaten humans [1–3]. Solar energy is a green, renewable, non-polluting and abundant energy source [4–10]. Although hydrogen is a clean energy which can be generated from photocatalytic splitting of water, the power conversion efficiency is lower rather than it is in applications [11–15]. Photocatalytic water splitting on TiO_2 photoelectrode is first reported by Fujishima and Honda [16], which opens up a new way to produce hydrogen. Up to now, many semiconductor materials, including g-C_3N_4, CdS, TiO_2 and CoP, have been developed to be used as photocatalysts for H_2 production [17–27].

Among the above photocatalysts, g-C_3N_4 has received much attention. It has some unique characteristics, such as metal free, non-toxic, simpler synthesis and suitable band gap [28–36]. The basic mechanism of g-C_3N_4 photocatalysis is as shown in Fig. 1. For the thermodynamic requirement, the location of conduction band (CB) and valence band (VB) for g-C_3N_4 is suitable for reducing water to produce H_2, because CB bottom g-C_3N_4 (−1.3 V vs. NHE) is lower than the electrode potential (0 V vs. NHE). Unfortunately, its activity is quite low, due to its low visible light absorption and the low recombination efficiency of charge separation. At present, various methods have been developed to enhance its photocatalytic activity of g-C_3N_4, which include doping ion, heterojunction design, copolymerization, loading noble metal, etc. [37–44]. In above methods, loading noble metals, including Pt, Ag, Pd or Au, is a very useful way to improve the photocatalytic performance of g-C_3N_4. Particularly, Pt enhances photocatalytic activity of H_2-generation for g-C_3N_4 since Pt can reduce the over potential as well as activation energy in the process of H^+ reducing to H_2. Also Pt

* Corresponding authors.

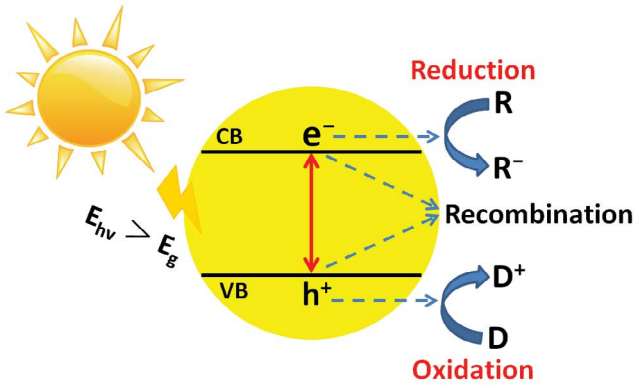

Fig. 1. Basic photocatalytic mechanism of g-C_3N_4. E_{hv} is the irradiated photon energy, *R* is the electron acceptor and *D* is the electron donor.

can capture electrons from g-C_3N_4 and increase the charge separation efficiency [45–47].

Herein, a facile method is reported to synthesize the g-C_3N_4/Pt composites using for photocatalytic H_2-production. The g-C_3N_4 nanosheets are synthesized via polymerization of urea and Pt/g-C_3N_4 composites are prepared through coating of Pt nanoparticles (NPs) on g-C_3N_4 surfaces by a liquid-phase reduction method. These prepared Pt/g-C_3N_4 composites are used as photocatalysts, showing an enhanced photocatalytic activity for H_2-production. Pt/g-C_3N_4 with 3 wt.% loading amount of Pt exhibits the highest photocatalytic activity among them. The enhanced photocatalytic performance is because loading Pt NPs effectively reduces the recombination of photogenerated electron–hole (e^--h^+) pairs. This research reported a facile method for preparing Pt/g-C_3N_4 composites, which may help to develop high activity photocatalysts for H_2 generation.

2. Experimental

2.1. Syntheses

The g-C_3N_4 materials are synthesized through direct heating of urea at 500°C with the heating rate of 10°C min^{-1}, then maintaining for 5 h. After the reaction, it cooled down to ambient temperature naturally. These Pt/g-C_3N_4 composites are synthesized via a liquid-phase reduction method. 0.5 g of g-C_3N_4 is put into 50 mL of water and ultrasonic treated for 5 min. Second, different amounts of $H_2PtCl_6{\cdot}6H_2O$ (1 g L^{-1}) aqueous solution is put into the above solution and stirring was maintained. Third, a certain amount of $NaBH_4$ was dissolved in 30 mL of water (the molar ratio of $n(H_2PtCl_6)$:$n(NaBH_4)$ = 1:5), and then put into the above solution, stirring for 1 h. Finally, the product is centrifuged and washed with absolute ethanol and distilled water, respectively, dried at 70°C for 5 h in vacuum oven. By different loading of Pt NPs, various ratio of (m[Pt]:n[g-C_3N_4] = 1%, 2%, 3%, 4% and 5%) Pt/g-C_3N_4 composites are synthesized and named as 1%-Pt/g-C_3N_4, 2%-Pt/g-C_3N_4, 3%-Pt/g-C_3N_4, 4%-Pt/g-C_3N_4 and 5%-Pt/g-C_3N_4, respectively.

2.2. Characterization

The crystal phase of the as-synthesized samples is investigated by X-ray diffraction (XRD, Bruker D5005 X-ray diffractometer, Cu Kα radiation source, λ = 1.54056 Å). Fourier transform infrared (FTIR) spectra are recorded on a Nicolet Magna 560 spectrophotometer. The morphology of samples is observed by high resolution transmission electron microscopy (HRTEM, JEOL JEM-2100F, Japan). UV–Vis diffuse reflectance spectra are recorded on a Shimadzu UV-3100 (Japan) spectrophotometer, with a $BaSO_4$ reference standard. X-ray photoelectron spectroscopy (XPS, PHI Quantum 1600, Japan) measurements are conducted to examine the surface chemical composition. Photoluminescence (PL) spectra excited at 325 nm are recorded on a Varian Cary Eclipse spectrometer.

2.3. Photocatalytic splitting

The photocatalytic H_2 production is conducted in a 100 mL Pyrex flask with closed system. A 350 W Xe lamp is used as the simulated sunlight source. 10 mg photocatalyst was put into 70 mL water with 10 mL triethanolamine as the sacrificial reagent. Before irradiation, the above reaction solution is aerated by using N_2 for 30 min to remove the dissolved oxygen. Under irradiation, the reaction solution is undertaken continuous stirring to keep photocatalysts effective suspension. The generation of H_2 is analyzed by using a Shimadzu GC-14C gas chromatograph.

2.4. Photoelectrochemical test

The transient photocurrent is investigated on a CHI660D electrochemical work station using a standard three-electrode system. 5 mg g-C_3N_4 or Pt/g-C_3N_4 is dispersed in 1 mL ethanol to get slurry. The working electrode is prepared by putting the obtained slurry on the ITO glass substrate (2 cm × 4 cm). A Pt wire is used as the counter electrode, and a calomel electrode as the reference. The electrolyte is 0.1 M aqueous Na_2SO_4 solution. The electrochemical impedance spectroscopy (EIS) Nyquist plots are obtained with an amplitude of 5 mV in the frequency range from 10^5 to 1 Hz at an open potential.

3. Results and discussion

3.1. XRD

Fig. 2 shows the XRD patterns of as-prepared samples. All the samples have two peaks at 13.1° and 27.5°, which are assigned to (100) and (002) of g-C_3N_4 (JCPDS 87-1526) [48]. The relative intensity of peak at 27.5° is weaker with increasing the loading amount of Pt on g-C_3N_4. No obvious reflection related to Pt is found due to the low amount and the high dilution effect of Pt NPs on the surface of g-C_3N_4 [49].

3.2. FTIR

The FTIR spectra of pure g-C_3N_4 nanosheets and Pt/g-C_3N_4 composites are as shown in Fig. 3. The peak at 1,639 cm^{-1} belongs to the skeletal aromatic vibration C–N. The peaks at 1,249, 1,319 and 1,433 cm^{-1} are associated with the C–N stretching vibration [50]. The peak at 804 cm^{-1} represents the typical breathing mode of the triazine units [51].

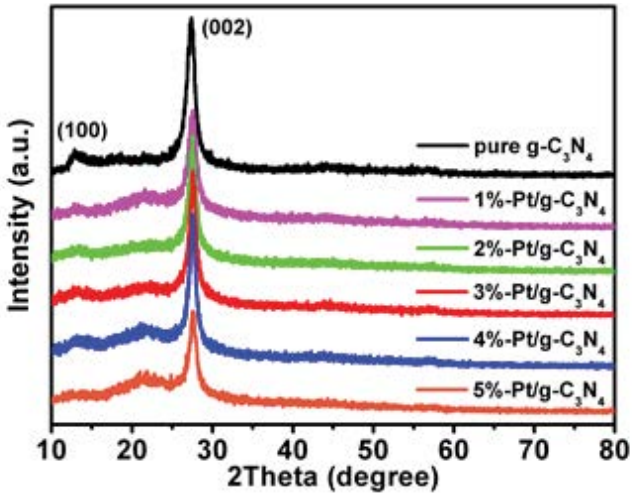

Fig. 2. XRD patterns of pure g-C_3N_4 and Pt/g-C_3N_4 samples.

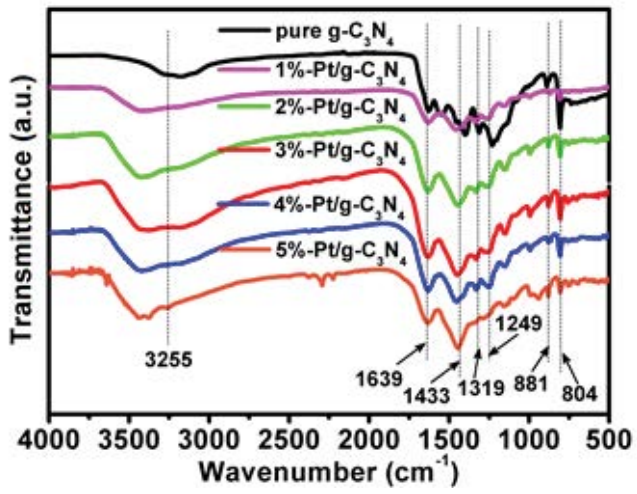

Fig. 3. FTIR spectra of pure g-C_3N_4 and Pt/g-C_3N_4 samples.

The broad peak at 3,255 cm^{-1} is attributed to the residual N–H groups [52]. It is found that there are no obvious changes for the characteristic FTIR peaks, meaning that the overall original structure of g-C_3N_4 is not changed by Pt NPs loading. It means that the Pt NPs are just adsorbed on g-C_3N_4 surfaces, agreeing well with the XRD result.

3.3. UV–Vis DRS

The UV–DRS measurement is used to study the optical adsorption property and the band structure of the as-prepared samples (Fig. 4). The pure g-C_3N_4 nanosheet shows a light absorption edge at 440 nm, which is consistent to its intrinsic band gap of bulk g-C_3N_4 [53]. The Pt/g-C_3N_4 composite exhibits a similar light absorption range compared with that pure g-C_3N_4, but the visible light adsorption is enhanced with increasing amount of Pt loading. The background absorption is enhanced with Pt loading amount increasing in the visible light region, because of the localized surface plasmon resonance effect [54].

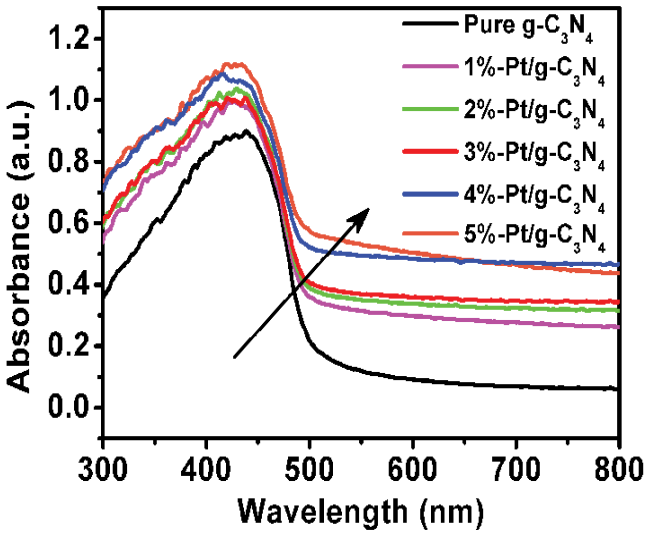

Fig. 4. UV–Vis DRS of pure g-C_3N_4 and Pt/g-C_3N_4 samples.

3.4. XPS

The surface chemical composition of Pt/g-C_3N_4 is studied by XPS, here 3%-Pt/g-C_3N_4 is selected for investigation. From the survey spectra of the both samples, the elements of C, O and N are observed, Pt is observed in 3%-Pt/g-C_3N_4 (Fig. 5a). The peaks at 284.6 and 288.0 eV are assigned to C 1s (Fig. 5b). The peaks at 284.6 and 288.0 eV are assigned to sp^2-hybridized carbon and carbon from N–C=N_2 coordination, respectively [55]. The N 1s peaks at 398.7, 399.8 and 401.0 eV are ascribed to sp^2-hybridized nitrogen of C–N–C, tertiary nitrogen of N–$(C)_3$ and amino functional C–N–H, respectively [48]. The peaks at 398.9, 400.1 and 401.2 eV for N 1s in pure g-C_3N_4 slightly moved to higher binding energies after Pt loading, as shown in Fig. 5c. The delocalized pi bond in g-C_3N_4 induce g-C_3N_4 has high electron density, which induce g-C_3N_4 can provide lone electron pairs and electrons transfer to *d* orbitals of Pt. Compared with pure g-C_3N_4, the shift in binding energy is observed in Pt/g-C_3N_4, indicating that Pt bonds with g-C_3N_4 strongly. For the Pt 4f XPS spectra (Fig. 5d), the two peaks are located at 71.11 and 74.30 eV, which are indexed as Pt 4f7/2 and Pt 4f5/2, respectively, indicating that Pt on g-C_3N_4 [54]. The splitting value is 3.19 eV between the two peaks, which also support the existence of metallic Pt [56]. The XPS result confirms the presence of Pt NPs on the surface of g-C_3N_4.

3.5. TEM

The TEM measurement is used to study the morphology of pure g-C_3N_4 and 3%-Pt/g-C_3N_4 samples. The TEM image of 3%-Pt/g-C_3N_4 (Fig. 6a) shows that Pt NPs are observed as black dots and dispersed on the g-C_3N_4 surface uniformly. The size of Pt NPs is in range from 4 to 8 nm, indicating that the Pt NPs are Pt clusters [57]. The HRTEM image demonstrates that the Pt NPs strongly bind to g-C_3N_4 (Fig. 6b), and the interplanar distance of Pt is 0.215 nm, which is assigned to the Pt (111) plane. The above TEM analysis confirms that these Pt NPs uniformly adsorb on g-C_3N_4 surface.

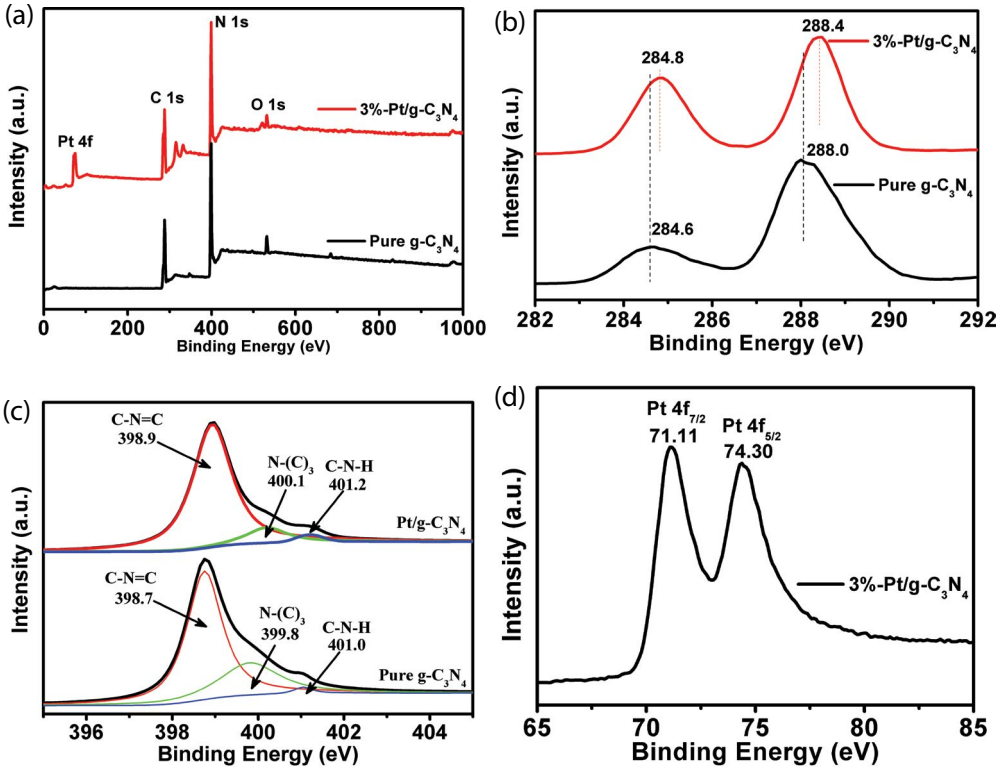

Fig. 5. XPS spectra of 3%-Pt/g-C_3N_4 composites: (a) survey XPS spectrum; high resolution of (b) C1s spectra; (c) N1s spectrum and (d) Pt 4f spectrum.

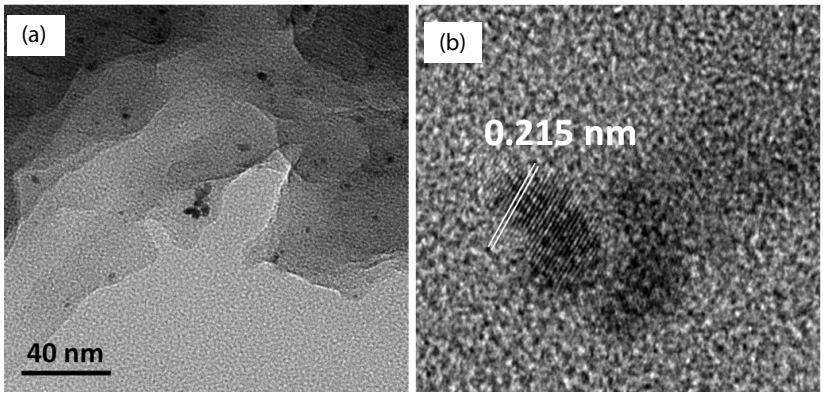

Fig. 6. TEM (a) and HRTEM (b) images of 3%-Pt/g-C_3N_4.

3.6. Photocatalytic performance

The photocatalytic activity of Pt/g-C_3N_4 composites is studied by photocatalytic H_2-generation (Fig. 7). The photocatalytic H_2-generation rate is very low for pure g-C_3N_4, almost no hydrogen production. After modification by Pt, the rate of hydrogen production is enhanced for g-C_3N_4. When Pt loading amounts is up to 3 wt.%, 3%-Pt/g-C_3N_4 shows the best photocatalytic performance of water splitting for hydrogen production (841 μmol g^{-1} h^{-1}) among these as-prepared samples. When the loading amount of Pt increases to 5 wt.%, the hydrogen evolution rate is declined to 665 μmol g^{-1} h^{-1}. This excessive loading of Pt causes a weaker photocatalytic activity, which is due to the excess Pt clusters working as recombination centers, or the active site is covered. A similar phenomenon was observed in photocatalytic reduction of CO_2 to produce CH_4 over Pt/g-C_3N_4 [58]. Thus, loading appropriate amount of Pt NPs on the g-C_3N_4 surface is a key point to ensure the high photocatalytic activity for H_2-generation.

3.7. Hydroxyl radical generation

The reaction of terephthalic acid (TA) to 2-hydroxyterephthalic acid (TAOH) is an useful method to study the efficiency of hydroxyl radical (•OH) generation [59]. In this

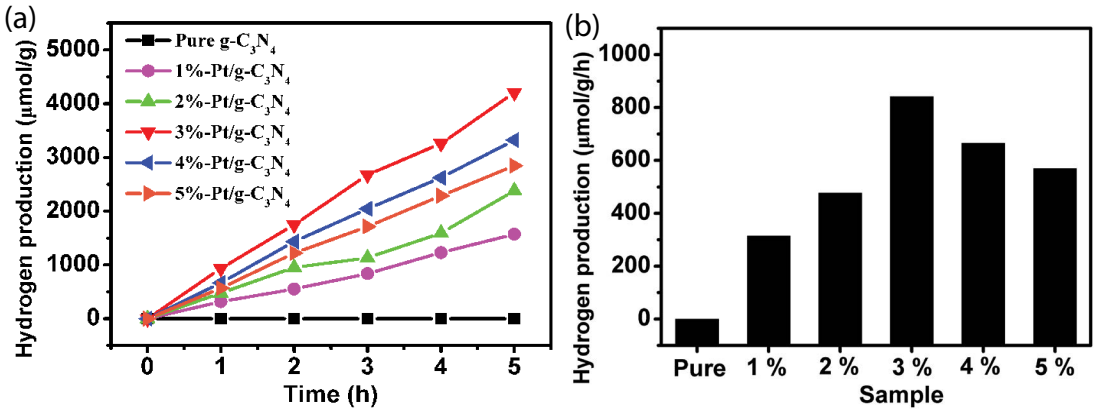

Fig. 7. (a) Plots of photocatalytic H_2-generation amount simulated sunlight irradiation time and (b) comparison of hydrogen evolution rate for different loading amount of Pt on g-C_3N_4 photocatalysts.

work, the reaction solution is made up of 3 mmol L^{-1} TA and 10 mmol L^{-1} NaOH. Under irradiation, TA can react with •OH and form TAOH, TAOH can generate fluorescence at an emission band at λ_{max} = 425 nm by excited light of λ_{exc} = 315 nm. TA to TAOH is tested to check the efficiency of •OH generation between pure g-C_3N_4 and 3%-Pt/g-C_3N_4, meaning to check the h^+ generation rate. It is known that •OH generation from h^+ react with OH^-. With simulated sunlight irradiation, the TAOH concentration is monitored within 30 min, every 5 min one sample is taken (Fig. 8). Comparing with that of pure g-C_3N_4, 3%-Pt/g-C_3N_4 demonstrates a higher generation rate of •OH, due to loading of Pt NPs on the g-C_3N_4 surface promotes the separation efficiency of photogenerated e^--h^+ pairs.

3.8. PL spectra

The excess energy of excited electrons can be released by three ways: emitted as PL, photogenerated e^--h^+ recombination, and thermal energy dissipation. Thus, PL measurement is carried out to study the separation efficiency of photogenerated e^--h^+ pairs. Fig. 9 illustrates that all

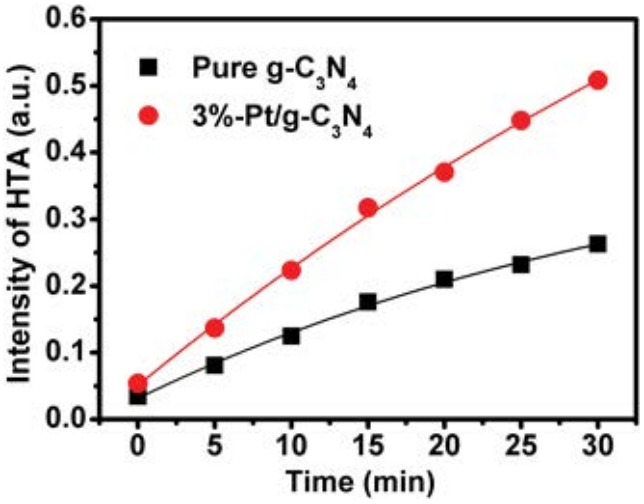

Fig. 8. TA react with •OH to TAOH generation by simulated solar irradiation.

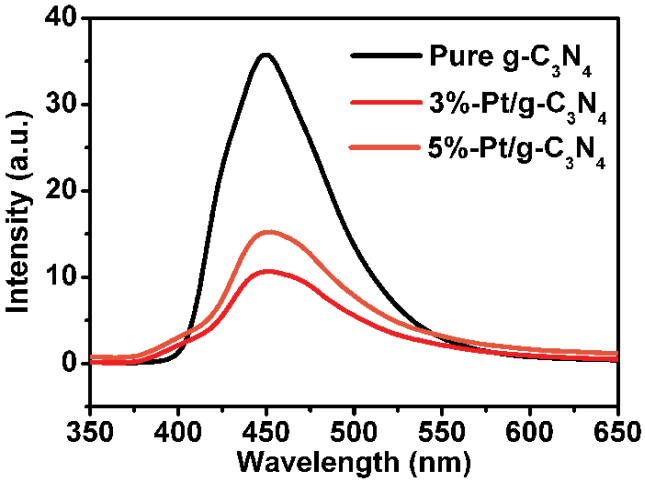

Fig. 9. PL spectra of pure g-C_3N_4, 3%-Pt/g-C_3N_4 and 5%-Pt/g-C_3N_4 samples.

the samples present an emission peak at ca. 460 nm. After loading of Pt NPs, the PL intensity of g-C_3N_4 reduces clearly. The weaker peak intensity of PL results in the relay effect of the cocatalyst Pt for the excited electrons, which diminishes the recombination rate of photogenerated carriers [49]. This improved separation of e^- and h^+ pairs can speed up the water splitting process. Thus, the Pt/g-C_3N_4 composites have a potential to be used as photocatalysts with high activity. However, over loading of Pt on g-C_3N_4, for example, 5%-Pt/g-C_3N_4, the PL intensity is increasing and stronger than that of 3%-Pt/g-C_3N_4, which indicates an increasing combination of photogenerated carriers [54]. Thus the suitable content of loading Pt NPs is a key point on improving the photocatalytic performance of g-C_3N_4.

3.9. Photoelectrochemical property

The photogenerated e^--h^+ separation efficiency of photocatalysts is investigated under simulated sunlight irradiation by the photoelectrochemical measurements. The photocurrent disappeared when the light was turned off, and restarted when the light was turned on (Fig. 10a). The

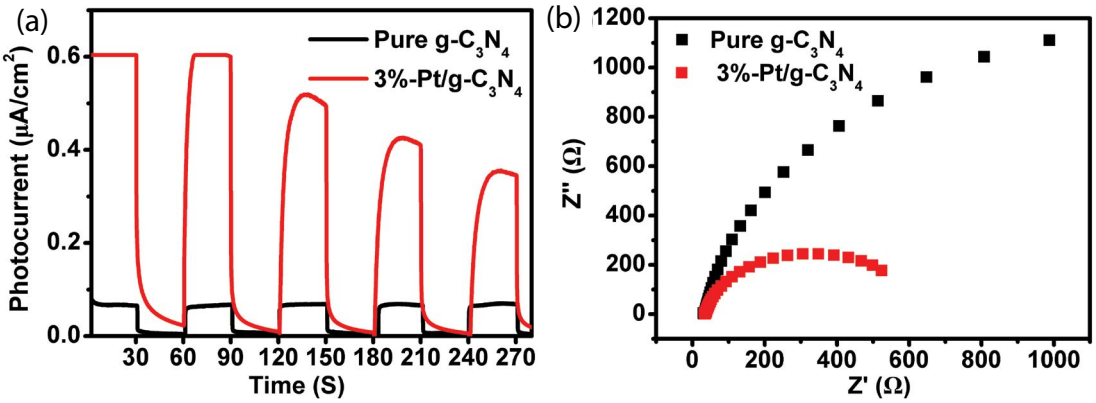

Fig. 10. (a) Photocurrent response and (b) electrochemical impedance spectroscopy of pure g-C_3N_4 and 3%-Pt/g-C_3N_4 samples.

3%-Pt/g-C_3N_4 samples show a little decrease for the reproducible photocurrent responses during the four turn off and turn on of the light. The photocurrent density of 3%-Pt/g-C_3N_4 with 0.7–1.2 μA cm^{-2} is stronger than that of pure g-C_3N_4 with ~0.1 μA cm^{-2}, which is due to the higher separation rate of photogenerated carriers in Pt/g-C_3N_4. This more efficient separation of photoinduced e^-/h^+ pairs in Pt/g-C_3N_4 is consistent with its higher H_2-evolution rate.

In order to further study the charge separation, the EIS Nyquist plots is used, as shown in Fig. 10b. The previous report suggested that the smaller arc radius of EIS Nyquist plots, the higher charge-transfer rate [60]. The radius on the EIS Nyquist plot of 3%-Pt/g-C_3N_4 is smaller than that of pure g-C_3N_4, indicating that Pt modification could reduce the charge recombination and promote the photogenerated e^--h^+ separation in g-C_3N_4, agreeing well with PL spectra and H_2-generation data.

3.10. Photocatalytic mechanism of water splitting

Fig. 11 shows a proposed mechanism of Pt/g-C_3N_4 during the photocatalytic H_2-generation. When Pt/g-C_3N_4 is under simulated sunlight irradiation, electrons can be excited to g-C_3N_4 CB, and holes leave at VB. The CB edge of g-C_3N_4 (−3.08 eV vs. vacuum) is higher that Fermi level of Pt (−5.1 eV vs. vacuum) [61]. Thus, the excited electrons on the g-C_3N_4 CB will surmount the Schottky barrier and escape to the Fermi energy level (E_f) of Pt, causing the increase separation of e^--h^+ pairs. The coordination of bands between g-C_3N_4 and Pt will increase the conductivity of g-C_3N_4, and enhance electrons escape from g-C_3N_4 to Pt. In this process, the electrons transfer from the g-C_3N_4 to Pt contribute to the Pt Fermi level shifts to the more negative potential [62]. Thus, Pt owes a lower activation potential and higher electron density, which provides more opportunities to join the reaction of H^+ to H_2. With increasing the loading amount of Pt from 0 to 3 wt.%, the face touching surface area between g-C_3N_4 and Pt NPs is also increasing, which can speed up the electron transformation and speed up the separation rate of e^--h^+ pairs. However, too much loading amount of Pt NPs will contribute to an increased Schottky barrier, which can increase e^--h^+ recombination rate.

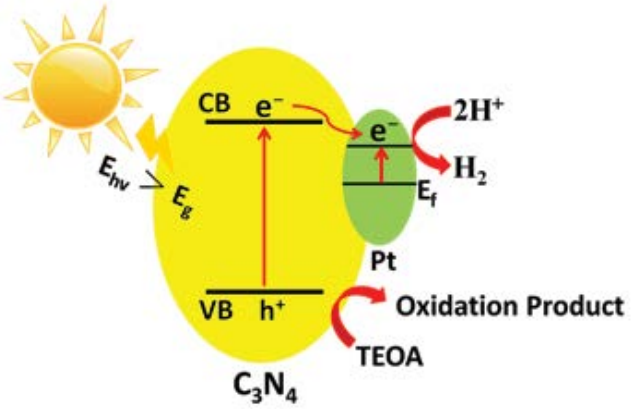

Fig. 11. Photocatalytic mechanism of water splitting for hydrogen generation over Pt/g-C_3N_4 composites.

4. Conclusions

Pt/g-C_3N_4 composites are successfully prepared in this work by using a simple liquid-phase reduction method. These Pt NPs uniformly adsorb on the surface of g-C_3N_4, with the size of 8–10 nm. After Pt loading, the Pt/g-C_3N_4 composites expand the visible light response and have enhanced photocatalytic H_2 generation under sunlight irradiation, especially for 3 wt Pt % loading, had the highest catalytic rate of H_2 generation (841 μmol g^{-1} h^{-1}), however, almost no hydrogen generation for pure g-C_3N_4. The photocatalytic activity of g-C_3N_4 is remarkably enhanced after Pt loading, because it enhances the visible-light response and suppresses the recombination of e^--h^+ pairs. This work indicates that the Pt/g-C_3N_4 composite is one of promising photocatalysts for hydrogen production.

Conflicts of interest

The authors declare no competing financial interest.

Acknowledgements

This work was supported by the National Natural Science Foundation of China (51602207), 111 project, Doctoral Scientific Research Foundation of Liaoning Province

(20170520011), Program for Liaoning Excellent Talents in University (LR2017074), and Project of Education Office of Liaoning Province (LQN201712).

References

[1] A.J. Esswein, D.G. Nocera, Hydrogen production by molecular photocatalysis, Chem. Rev., 107 (2007) 4022–4047.

[2] Z. Wei, Y. Zhang, S. Wang, C. Wang, J. Ma, Fe-doped phosphorene for the nitrogen reduction reaction, J. Mater. Chem. A, 6 (2018) 13790–13796.

[3] B. Wang, J. Xia, L. Mei, L. Wang, Q. Zhang, Highly efficient and rapid lead(II) scavenging by the natural artemia cyst shell with unique three-dimensional porous structure and strong sorption affinity, ACS Sustain. Chem. Eng., 6 (2017) 1343–1351.

[4] Z. Yan, S. Gong, L. An, L. Yue, Z. Xu, Enhanced catalytic activity of graphene oxide/CeO_2 supported Pt toward HCHO decomposition at room temperature, React. Kinet. Mech. Catal., 124 (2018) 293–304.

[5] W. Zhang, W. Wang, H. Shi, Y. Liang, J. Fu, M. Zhu, Surface plasmon-driven photoelectrochemical water splitting of aligned ZnO nanorod arrays decorated with loading-controllable Au nanoparticles, Sol. Energy Mater. Sol. Cells, 180 (2018) 25–33.

[6] Y. Zhao, Y. Wei, X. Wu, H. Zheng, Z. Zhao, J. Liu, J. Li, Graphene-wrapped Pt/TiO_2 photocatalysts with enhanced photogenerated charges separation and reactant adsorption for high selective photoreduction of CO_2 to CH_4, Appl. Catal., B, 226 (2018) 360–372.

[7] G. Wang, X. Long, K. Qi, S. Dang, M. Zhong, S. Xiao, T. Zhou, Two-dimensional CdS/g-C_6N_6 heterostructure used for visible light photocatalysis, Appl. Surf. Sci., 471 (2019) 162–167.

[8] M. Khanahmadi, M. Hajaghazadeh, F. Nejatzadeh-Barandozi, F. Gholami-Borujeni, Photocatalytic oxidation process (UV-Fe_2O_3) efficiency for degradation of hydroquinone, Desal. Wat. Treat., 106 (2018) 305–311.

[9] J. Yu, Z. Chen, L. Zeng, Y. Ma, Z. Feng, Y. Wu, H. Lin, L. Zhao, Y. He, Synthesis of carbon-doped $KNbO_3$ photocatalyst with excellent performance for photocatalytic hydrogen production, Sol. Energy Mater. Sol. Cells, 179 (2018) 45–56.

[10] K. Qi, S. Karthikeyan, W. Kim, F.A. Marzouqi, I.S. Al-Khusaibi, Y. Kim, R. Selvaraj, Hydrothermal synthesis of SnS_2 nanocrystals for photocatalytic degradation of 2,4,6-trichlorophenol under white LED light irradiation, Desal. Wat. Treat., 92 (2017) 108–115.

[11] Q. Xiang, J. Yu, M. Jaroniec, Preparation and enhanced visible-light photocatalytic H_2-production activity of graphene/C_3N_4 composites, J. Phys. Chem. C, 115 (2011) 7355–7363.

[12] Q. Xu, B. Zhu, C. Jiang, B. Cheng, J. Yu, Constructing 2D/2D Fe_2O_3/g-C_3N_4 direct Z-scheme photocatalysts with enhanced H_2 generation performance, Solar RRL, 2 (2018) 1800006.

[13] J. Low, J. Yu, M. Jaroniec, S. Wageh, A.A. Al-Ghamdi, Heterojunction photocatalysts, Adv. Mater., 29 (2017) 1601694.

[14] F. Alexander, M. AlMheiri, P. Dahal, J. Abed, N.S. Rajput, C. Aubry, J. Viegas, M. Jouiad, Water splitting TiO_2 composite material based on black silicon as an efficient photocatalyst, Sol. Energy Mater. Sol. Cells, 180 (2018) 236–242.

[15] S. Liu, J. Zhou, Y. Lu, J. Su, Pulsed laser/electrodeposited $CuBi_2O_4$/$BiVO_4$ p-n heterojunction for solar water splitting, Sol. Energy Mater. Sol. Cells, 180 (2018) 123–129.

[16] A. Fujishima, K. Honda, Electrochemical photolysis of water at a semiconductor electrode, Nature, 238 (1972) 37–38.

[17] Q. Xu, B. Cheng, J. Yu, G. Liu, Making co-condensed amorphous carbon/g-C_3N_4 composites with improved visible-light photocatalytic H_2-production performance using Pt as cocatalyst, Carbon, 118 (2017) 241–249.

[18] X. Xiang, L. Chou, X. Li, Synthesis of PdS-CdSe@CdS-Au nanorods with asymmetric tips with improved H_2 production efficiency in water splitting and increased photostability, Chin. J. Catal., 39 (2018) 407–412.

[19] S. Cao, Q. Huang, B. Zhu, J. Yu, Trace-level phosphorus and sodium co-doping of g-C_3N_4 for enhanced photocatalytic H_2 production, J. Power Sources, 351 (2017) 151–159.

[20] J. Fu, B. Zhu, W. You, M. Jaroniec, J. Yu, A flexible bio-inspired H_2-production photocatalyst, Appl. Catal., B, 220 (2018) 148–160.

[21] K. Qi, S.-y. Liu, M. Qiu, Photocatalytic performance of TiO_2 nanocrystals with/without oxygen defects, Chin. J. Catal., 39 (2018) 867–875.

[22] X. Li, R. Shen, S. Ma, X. Chen, J. Xie, Graphene-based heterojunction photocatalysts, Appl. Surf. Sci., 430 (2018) 53–107.

[23] K. Qi, B. Cheng, J. Yu, W. Ho, A review on TiO_2-based Z-scheme photocatalysts, Chin. J. Catal., 38 (2017) 1936–1955.

[24] R. Shen, C. Jiang, Q. Xiang, J. Xie, X. Li, Surface and interface engineering of hierarchical photocatalysts, Appl. Surf. Sci., 471 (2019) 43–87.

[25] Z. Yan, Z. Yang, Z. Xu, L. An, F. Xie, J. Liu, Enhanced room-temperature catalytic decomposition of formaldehyde on magnesium-aluminum hydrotalcite/boehmite supported platinum nanoparticles catalyst, J. Colloid Interface Sci., 524 (2018) 306–312.

[26] K. Qi, B. Cheng, J. Yu, W. Ho, Review on the improvement of the photocatalytic and antibacterial activities of ZnO, J. Alloys Compd., 727 (2017) 792–820.

[27] K. Qi, S.-y. Liu, Y. Chen, B. Xia, G.-D. Li, A simple post-treatment with urea solution to enhance the photoelectric conversion efficiency for TiO_2 dye-sensitized solar cells, Sol. Energy Mater. Sol. Cells, 183 (2018) 193–199.

[28] J. Fu, J. Yu, C. Jiang, B. Cheng, g-C_3N_4-based heterostructured photocatalysts, Adv. Energy Mater., 8 (2018) 1701503.

[29] B. Zhu, L. Zhang, B. Cheng, J. Yu, First-principle calculation study of tri-*s*-triazine-based g-C_3N_4: a review, Appl. Catal., B, 224 (2018) 983–999.

[30] K. Qi, Y. Xie, R. Wang, S.-y. Liu, Z. Zhao, Electroless plating Ni-P cocatalyst decorated g-C_3N_4 with enhanced photocatalytic water splitting for H_2 generation, Appl. Surf. Sci., 466 (2019) 847–853.

[31] J. Wen, J. Xie, X. Chen, X. Li, A review on g-C_3N_4-based photocatalysts, Appl. Surf. Sci., 391 (2017) 72–123.

[32] H. Yang, Z. Jin, H. Hu, Y. Bi, G. Lu, Ni-Mo-S nanoparticles modified graphitic C_3N_4 for efficient hydrogen evolution, Appl. Surf. Sci., 427 (2018) 587–597.

[33] W. Yu, J. Chen, T. Shang, L. Chen, L. Gu, T. Peng, Direct Z-scheme g-C_3N_4/WO_3 photocatalyst with atomically defined junction for H_2 production, Appl. Catal., B, 219 (2017) 693–704.

[34] M. Wu, J. Zhang, C. Liu, Y. Gong, R. Wang, B. He, H. Wang, Rational design and fabrication of noble-metal-free Ni_xP cocatalyst embedded 3D N-TiO_2/g-C_3N_4 heterojunctions with enhanced photocatalytic hydrogen evolution, Chem. Cat. Chem., 10 (2018) 3069–3077.

[35] T. Song, P. Zhang, J. Zeng, T. Wang, A. Ali, H. Zeng, In situ construction of globe-like carbon nitride as a self-cocatalyst modified tree-like carbon nitride for drastic improvement in visible-light photocatalytic hydrogen evolution, Chem. Cat. Chem., 9 (2017) 4035–4042.

[36] Z. Zhang, Y. Zhang, L. Lu, Y. Si, S. Zhang, Y. Chen, K. Dai, P. Duan, L. Duan, J. Liu, Graphitic carbon nitride nanosheet for photocatalytic hydrogen production: the impact of morphology and element composition, Appl. Surf. Sci., 391 (2017) 369–375.

[37] S. Cao, J. Low, J. Yu, M. Jaroniec, Polymeric photocatalysts based on graphitic carbon nitride, Adv. Mater., 27 (2015) 2150–2176.

[38] R. Shen, J. Xie, X. Lu, X. Chen, X. Li, Bifunctional Cu_3P decorated g-C_3N_4 nanosheets as a highly active and robust visible-light photocatalyst for H_2 production, ACS Sustain. Chem. Eng., 6 (2018) 4026–4036.

[39] R. Shen, J. Xie, H. Zhang, A. Zhang, X. Chen, X. Li, Enhanced solar fuel H_2 generation over g-C_3N_4 nanosheet photocatalysts by the synergetic effect of noble metal-free Co_2P cocatalyst and the environmental phosphorylation strategy, ACS Sustain. Chem. Eng., 6 (2017) 816–826.

[40] J. Fu, Q. Xu, J. Low, C. Jiang, J. Yu, Ultrathin 2D/2D WO_3/g-C_3N_4 step-scheme H_2-production photocatalyst, Appl. Catal., B, 243 (2019) 556–565.

[41] M.S. Akple, J. Low, S. Wageh, A.A. Al-Ghamdi, J. Yu, J. Zhang, Enhanced visible light photocatalytic H_2-production of g-C_3N_4/

WS_2 composite heterostructures, Appl. Surf. Sci., 358 (2015) 196–203.
[42] P. Xia, M. Liu, B. Cheng, J. Yu, L. Zhang, Dopamine modified g-C_3N_4 and its enhanced visible-light photocatalytic H_2-production activity, ACS Sustain. Chem. Eng., 6 (2018) 8945–8953.
[43] F. Al Marzouqi, R. Selvaraj, Y. Kim, Thermal oxidation etching process of g-C_3N_4 nanosheets from their bulk materials and its photocatalytic activity under solar light irradiation, Desal. Wat. Treat., 116 (2018) 267–276.
[44] N. Li, J. Zhou, Z. Sheng, W. Xiao, Molten salt-mediated formation of g-C_3N_4-MoS_2 for visible-light-driven photocatalytic hydrogen evolution, Appl. Surf. Sci., 430 (2018) 218–224.
[45] X. Chen, Y.-S. Jun, K. Takanabe, K. Maeda, K. Domen, X. Fu, M. Antonietti, X. Wang, Ordered mesoporous SBA-15 type graphitic carbon nitride: a semiconductor host structure for photocatalytic hydrogen evolution with visible light, Chem. Mater., 21 (2009) 4093–4095.
[46] J. Xu, L. Zhang, R. Shi, Y. Zhu, Chemical exfoliation of graphitic carbon nitride for efficient heterogeneous photocatalysis, J. Mater. Chem. A, 1 (2013) 14766–14772.
[47] M. Liu, P. Xia, L. Zhang, B. Cheng, J. Yu, Enhanced photocatalytic H_2-production activity of g-C_3N_4 nanosheets via optimal photodeposition of Pt as cocatalyst, ACS Sustain. Chem. Eng., 6 (2018) 10472–10480.
[48] Q. Lin, L. Li, S. Liang, M. Liu, J. Bi, L. Wu, Efficient synthesis of monolayer carbon nitride 2D nanosheet with tunable concentration and enhanced visible-light photocatalytic activities, Appl. Catal., B, 163 (2015) 135–142.
[49] Z. Lu, W. Song, C. Ouyang, H. Wang, D. Zeng, C. Xie, Enhanced visible-light photocatalytic performance of highly-dispersed Pt/g-C_3N_4 nanocomposites by one-step solvothermal treatment, RSC Adv., 7 (2017) 33552–33557.
[50] S. Huang, Y. Xu, M. Xie, H. Xu, M. He, J. Xia, L. Huang, H. Li, Synthesis of magnetic $CoFe_2O_4$/g-C_3N_4 composite and its enhancement of photocatalytic ability under visible-light, Colloids Surf., A, 478 (2015) 71–80.
[51] J.-X. Sun, Y.-P. Yuan, L.-G. Qiu, X. Jiang, A.-J. Xie, Y.-H. Shen, J.-F. Zhu, Fabrication of composite photocatalyst g-C_3N_4–ZnO and enhancement of photocatalytic activity under visible light, Dalton Trans., 41 (2012) 6756–6763.
[52] S. Cao, Y. Li, B. Zhu, M. Jaroniec, J. Yu, Facet effect of Pd cocatalyst on photocatalytic CO_2 reduction over g-C_3N_4, J. Catal., 349 (2017) 208–217.
[53] W.-J. Ong, L.-L. Tan, S.-P. Chai, S.-T. Yong, A.R. Mohamed, Surface charge modification via protonation of graphitic carbon nitride (g-C_3N_4) for electrostatic self-assembly construction of 2D/2D reduced graphene oxide (rGO)/g-C_3N_4 nanostructures toward enhanced photocatalytic reduction of carbon dioxide to methane, Nano Energy, 13 (2015) 757–770.
[54] W.-J. Ong, L.-L. Tan, S.-P. Chai, S.-T. Yong, Heterojunction engineering of graphitic carbon nitride (g-C_3N_4) via Pt loading with improved daylight-induced photocatalytic reduction of carbon dioxide to methane, Dalton Trans., 44 (2015) 1249–1257.
[55] F. Li, Z. Yu, H. Shi, Q. Yang, Q. Chen, Y. Pan, G. Zeng, L. Yan, A Mussel-inspired method to fabricate reduced graphene oxide/g-C_3N_4 composites membranes for catalytic decomposition and oil-in-water emulsion separation, Chem. Eng. J., 322 (2017) 33–45.
[56] W. Kim, T. Tachikawa, H. Kim, N. Lakshminarasimhan, P. Murugan, H. Park, T. Majima, W. Choi, Visible light photocatalytic activities of nitrogen and platinum-doped TiO_2: Synergistic effects of co-dopants, Appl. Catal., B, 147 (2014) 642–650.
[57] R. Nazir, P. Fageria, M. Basu, S. Gangopadhyay, S. Pande, Decoration of Pd and Pt nanoparticles on a carbon nitride (C_3N_4) surface for nitro-compounds reduction and hydrogen evolution reaction, New J. Chem., 41 (2017) 9658–9667.
[58] J. Yu, K. Wang, W. Xiao, B. Cheng, Photocatalytic reduction of CO_2 into hydrocarbon solar fuels over g-C_3N_4–Pt nanocomposite photocatalysts, Phys. Chem. Chem. Phys., 16 (2014) 11492–11501.
[59] T. Hirakawa, Y. Nosaka, Properties of $O^{2-\bullet}$ and $OH^{\bullet}$ formed in TiO_2 aqueous suspensions by photocatalytic reaction and the influence of H_2O_2 and some ions, Langmuir, 18 (2002) 3247–3254.
[60] M. Li, L. Zhang, X. Fan, Y. Zhou, M. Wu, J. Shi, Highly selective CO_2 photoreduction to CO over g-C_3N_4/Bi_2WO_6 composites under visible light, J. Mater. Chem. A, 3 (2015) 5189–5196.
[61] H.-S. Wu, L.-D. Sun, H.-P. Zhou, C.-H. Yan, Novel TiO_2–Pt@SiO_2 nanocomposites with high photocatalytic activity, Nanoscale, 4 (2012) 3242–3247.
[62] G. Liu, K. Du, S. Haussener, K. Wang, Charge transport in two-photon semiconducting structures for solar fuels, ChemSusChem, 9 (2016) 2878–2904.